ACS APPLIED MATERIALS & INTERFACES

www.acsami.org

Research Article

Metal Silicidation in Conjunction with Dopant Segregation: A Promising Strategy for Fabricating High-Performance Silicon-Based Photoanodes

Shengyang Li, Guangwei She,* Jing Xu, Shaoyang Zhang, Haoyue Zhang, Lixuan Mu, Chen Ge, Kuijuan Jin, Jun Luo,* and Wensheng Shi*

Cite This: *ACS Appl. Mater. Interfaces* 2020, 12, 39092−39097

Read Online

ACCESS | Metrics & More | Article Recommendations | Supporting Information

ABSTRACT: Silicon (Si)-based Schottky junction photoelectrodes have attracted considerable attention for photoelectrochemical (PEC) water splitting in recent years. To realize highly efficient Si-based Schottky junction photoelectrodes, the critical challenge is to enable the photoelectrodes to not only have a high Schottky barrier height (SBH), by which a high photovoltage can be obtained, but also ensure an efficient charge transport. Here, we propose and demonstrate a strategy to fabricate a high-performance NiSi/n-Si Schottky junction photoanode by metal silicidation in conjunction with dopant segregation (DS). The metal silicidation produces photoanodes with a high-quality NiSi/Si interface without a disordered SiO_2 layer, which ensures highly efficient charge transport, and thus a high saturated photocurrent density of 33 mA cm^{-2} was attained for the photoanode. The subsequent DS gives the photoanodes a high SBH of 0.94 eV through the introduction of electric dipoles at the NiSi/n-Si interface. As a result, a high photovoltage and favorable onset potential of 1.03 V vs RHE was achieved. In addition, the strong alkali corrosion resistance of NiSi also endows the photoanode with a high stability during PEC operation in 1 M KOH. Our work provides a universal strategy to fabricate metal−silicide/Si Schottky junction photoelectrodes for high-performance PEC water splitting.

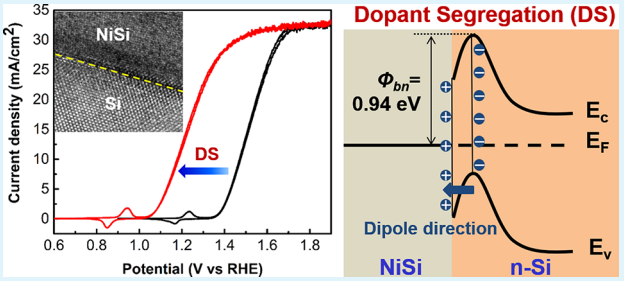

KEYWORDS: *silicon, metal silicidation, dopant segregation, photoanodes, water splitting*

INTRODUCTION

Silicon (Si)-based Schottky junction photoelectrodes have attracted considerable attention for photoelectrochemical (PEC) water splitting in recent years.[1−4] Depositing a thin layer of metal on Si to form a metal−semiconductor (MS) Schottky junction structure could not only protect the Si from corrosion but also catalyze the water-splitting reaction.[5,6] Nevertheless, the direct contact between the metal and Si can create metal-induced gap states on the Si surface, which unfortunately leads to a relatively low Schottky barrier height (SBH) through Fermi level pinning of Si, and thus a low photovoltage.[7,8] To realize a high SBH, as a current strategy, an insulator layer such as TiO_2, Al_2O_3, or high-quality thermal SiO_2 is inserted between the metal and semiconductor, which is known as the metal−insulator−semiconductor (MIS) architecture.[9−15] However, the insulator layer in the MIS structure also serves as a tunnel barrier for charge transfer.[4,16,17] Reportedly, the overpotential for water oxidation linearly increased at a rate of ∼21 mV nm^{-1} with increasing thickness of TiO_2 insulator layer.[18] In addition, for a Si-based MIS photoelectrode, the easy oxidation of Si causes the Si surface to inevitably form a disordered native SiO_2 layer during the deposition of the insulator layer.[19,20] This disordered SiO_2 layer results in a poor Si/SiO_2 interface.[21,22] Many efforts have concentrated on reducing the adverse effects of the insulator layers in MIS photoelectrodes.[4,23,24] Recently, Li et al. attempted to fully avoid the disordered SiO_2 layer on the Si surface of a MIS photocathode by epitaxially growing a thin $SrTiO_3$ layer on the p-Si surface via molecular beam epitaxy.[25] A peculiar configuration, the nearly perfect alignment between the conduction bands of the Si and $SrTiO_3$ enables the photoinduced electrons to be transported by the $SrTiO_3$ layer via band conduction instead of tunneling. However, it is irrational to extend such a configuration to n-Si for the fabrication of photoanodes because of the large valence band offset between the n-Si and $SrTiO_3$. Furthermore, there was still a small amount of Si suboxide between the $SrTiO_3$ and Si

Received: May 24, 2020
Accepted: August 11, 2020
Published: August 11, 2020

that resulted in a negative shift of the onset potential.[25] The adverse effects of the insulator layer could not be fully avoided, although the introduction of the insulator layer enhanced the SBH of the MS structure.

Therefore, realizing a high SBH from an MS structure without blocking the charge transfer is significant for high-performance Si-based Schottky junction photoelectrodes. Considering this point, here, we propose and demonstrate a strategy to fabricate high-performance NiSi/n-Si MS Schottky junction photoanode by metal silicidation in conjunction with dopant segregation (DS). The NiSi/n-Si structure can be obtained by the solid-state reaction between Ni and Si, known as metal silicidation.[26,27] Because of the absence of an insulator layer, the full avoidance of a disordered native SiO_2 layer, and the metallic nature of NiSi,[28] highly efficient charge transport was achieved, and thus a high saturated photocurrent density of 33 mA cm^{-2} was attained for the photoanode. The subsequent DS enhanced the SBH of NiSi/n-Si from 0.71 to 0.94 eV by introducing electrical dipoles at the NiSi/n-Si interface.[29−31] As a result, high photovoltage and favorable onset potential of 1.03 V vs RHE was achieved. In addition, the strong alkali corrosion resistance of NiSi enables the photoanode to have high stability during the PEC operation in alkaline solution. Because the metal silicidation in conjunction with the DS technique can also be applied to other metals (such as Co, Ir, and Pt) and Si, our work provides a universal strategy to fabricate metal−silicide/Si Schottky junction photoelectrodes for high-performance PEC water splitting.

EXPERIMENTAL DETAILS

Metal Silicidation. Single-side polished n-Si (phosphorus-doped, 1−10 Ω·cm, (100)-oriented, 450 μm thickness) wafers were used in this study. First, the Si wafers were cleaned using a standard RCA procedure consisting of immersing the wafers in RCA SC-1 and RCA SC-3 solutions successfully. Next, the wafers were soaked in a 5% HF solution for 10 s to remove the oxide layer. Finally, the wafers were rinsed using DI water and dried using a commercial spin rinse dryer in N_2. The cleaned Si wafers were immediately transferred to a magnetron sputtering chamber (ULVAC MLH-2306RDE). A 7 nm nickel film was sputtered on a silicon substrate through RF magnetron sputtering with a deposition rate of 4 nm/min. The wafer with a 7 nm Ni film was transferred into a rapid thermal process chamber (AG Associates Heatpulse 610) and annealed at 500 °C for 30 s under N_2 protection to obtain the NiSi/n-Si.

Dopant Segregation. Boron ions were implanted into the as-formed NiSi film at 5 keV with a tilt angle of 7°. The implantation dose is 1 × 10^{15} cm^{-2}. Subsequently, the specimen was annealed at 500 °C for 30 s in N_2 to drive the boron dopants to the NiSi/Si interface; finally, the DS-NiSi/n-Si was obtained.

PEC and Electrochemical Measurements. The photoelectrodes were packaged using previous methods.[32] All the PEC and electrochemical measurements were performed using a CHI660C workstation in a single-compartment square quartz glass electrochemical cell as shown in Figure S1. The active area of the photoelectrode is a circular region with a diameter of 7 mm. The electrolyte used for cyclic voltammetry (CV) and chronoamperometry measurements was 1 M KOH solution. The auxiliary electrode is an Hg/HgO electrode. The counter electrode is a Pt foil electrode. The as-prepared photoelectrodes were illuminated by a 500 W xenon lamp coupled with an AM 1.5 filter. Before each measurement, the light intensity was calibrated to 100 mW cm^{-2} using a calibrated reference Si solar cell (PVM955, PV Measurements) in air. The electrochemical impedance spectrum (EIS) was measured in an aqueous solution of 40 mM $K_3Fe(CN)_6$, 250 mM $K_4Fe(CN)_6$, and 1 M KCl (Note S1 in the Supporting Information).[22,33]

RESULTS AND DISCUSSION

Glancing angle XRD and micro-Raman spectroscopy (MRS) were used to demonstrate the formation of NiSi films. As shown in Figure 1a,b, the XRD peaks and the characteristic

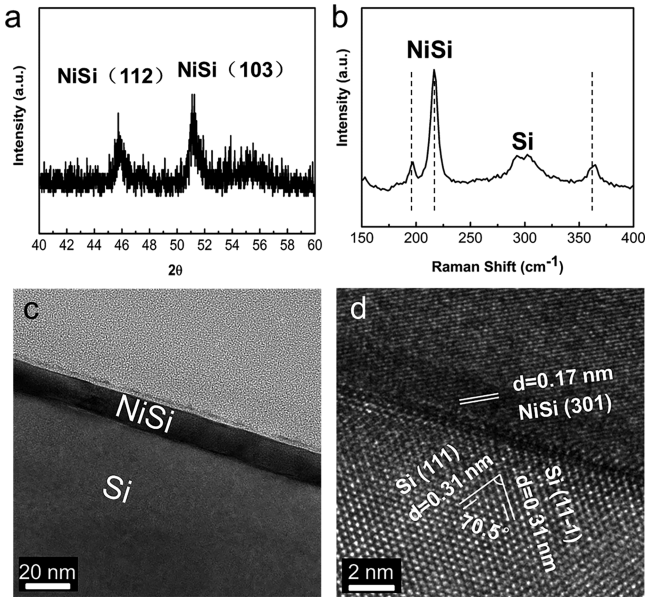

Figure 1. (a) XRD and (b) MRS of the NiSi film. (c) Cross-sectional TEM and (d) HRTEM of the NiSi/n-Si.

Raman scattering peaks of NiSi clearly reveal the formation of the NiSi film on Si.[34] The formation of the NiSi film can be attributed to the solid-state reaction between the outer layer Ni and Si at high temperature during the rapid thermal process.[26,27] The TEM image (Figure 1c) of NiSi/n-Si shows that the thickness of NiSi film is approximately 15 nm. The HRTEM image (Figure 1d) displays that the NiSi film was formed directly on the Si substrate with a perfect NiSi/Si interface and was free of a disordered SiO_2 layer. Because of the full avoidance of a disordered SiO_2 layer and the metallic nature of NiSi,[35] this structure is very favorable for charge transport as discussed below. The TEM images of NiSi/n-Si after the DS show that there are no obvious damages formed on the NiSi film during the DS (Figure S2).

EIS of the samples was performed to determine the SBH (ϕ_{bn}) of the NiSi/n-Si and DS-NiSi/n-Si. The Mott−Schottky plots (C^{2-}−V) of the NiSi/n-Si and DS-NiSi/n-Si all exhibit good linearity (Figure 2a,b). From the intercept of the fitted

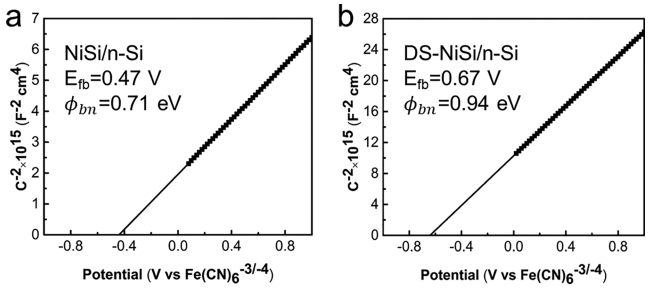

Figure 2. Mott−Schottky plots (C^{2-}−V) of the inverse square space charge capacitance as a function of applied voltage relative to the redox potential of $Fe(CN)_6^{3-/4-}$ for the NiSi/n-Si (a) and DS-NiSi/n-Si (b).

https://dx.doi.org/10.1021/acsami.0c09498
ACS Appl. Mater. Interfaces 2020, 12, 39092−39097

line with the x-axis, the flat band potential (E_{fb}) can be estimated. The E_{fb} values of the NiSi/n-Si without and with DS were 0.47 and 0.67 V, respectively. Accordingly, the SBH of the NiSi/n-Si and DS-NiSi/n-Si were determined to be 0.71 and 0.94 eV, respectively. The details of the calculation of the SBH were shown in Note S1 (Supporting Information). After the DS process, the SBH of NiSi/n-Si was increased by 230 meV. The higher SBH of DS-NiSi/n-Si was attributed to the electric dipoles introduced by the B DS at the NiSi/n-Si interface.[29,36] During the DS process, the B dopants were first implanted into the as-formed NiSi film. Upon subsequent drive-in annealing, because of the limited solubility of B in NiSi,[37] soluble B dopants could not be incorporated into the NiSi film and would instead tend to diffuse out of the NiSi film and finally accumulate at the NiSi/n-Si interface, where the B dopants partially substituted for the Si atoms on the Si lattice in close vicinity to the NiSi/n-Si interface.[29,31] Secondary ion-mass spectroscopy (SIMS) analysis was performed to profile the depth distribution of boron dopants in NiSi/n-Si after DS. As shown in Figure 3, the boron dopants accumulated at the

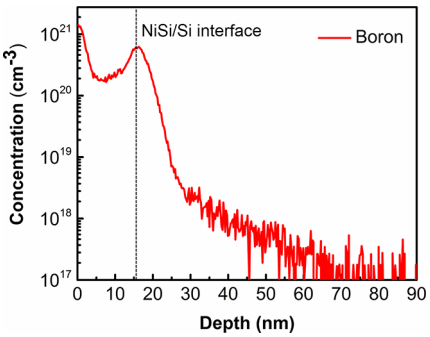

Figure 3. SIMS depth profiling of boron in DS-NiSi/n-Si.

NiSi/n-Si interface after DS. As a result, these substitutional B dopants were negatively charged, and the electric dipoles across the interface were consequently formed.[38] The electric dipoles caused the energy band to bend upward strongly, giving rise to an increase in the SBH.[36] Scheme 1 shows the energy band diagrams of NiSi/n-Si and DS-NiSi/n-Si and illustrates how the energy band of Si was bent upward by the electric dipoles.

Both the NiSi/n-Si and DS-NiSi/n-Si were used as photoanodes for PEC water splitting. The CV curves were measured without any iR compensation. Both electrodes were

Scheme 1. Energy Band Diagrams of the NiSi/n-Si and DS-NiSi/n-Si[a]

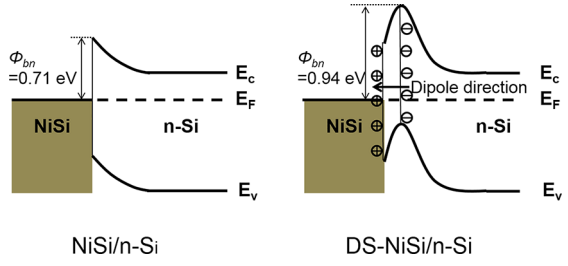

[a]The increase in SBH was due to the introduction of the electric dipoles, which made the energy band bend upward at the NiSi/n-Si interface.

cycled 60 times to activate the surfaces of the photoanodes until the stable CV curves were obtained. Figure 4a shows the

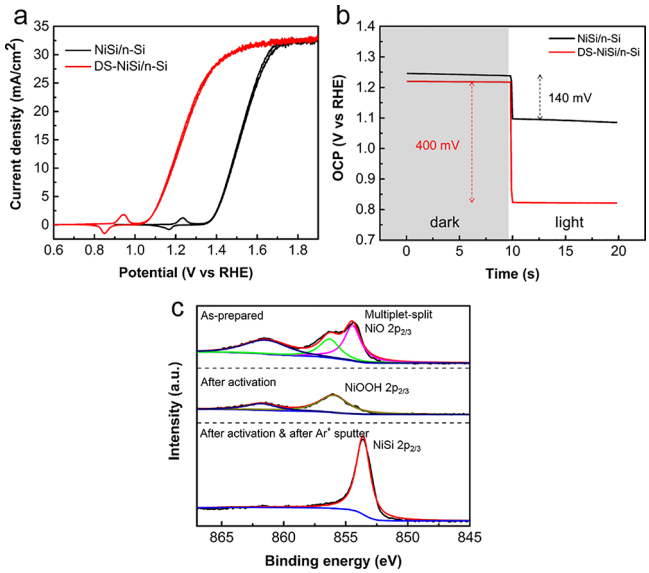

Figure 4. (a) CV curves of NiSi/n-Si (black) and DS-NiSi/n-Si (red) in 1 M KOH solution under simulated 100 mW cm^{-2} illumination. (b) Electrical open-circuit potential of NiSi/n-Si (black) and DS-NiSi/n-Si (red) in 1 M KOH solution measured in the dark and under illumination. The difference in the OCPs between the dark and illuminated conditions reflects the value of the photovoltage. (c) High-resolution Ni 2p$_{2/3}$ XPS spectra of NiSi/n-Si under different conditions: as-prepared, after activation (60 CV cycles in 1 M KOH solution), and after activation plus 30 s Ar$^+$ sputtering.

CV curves of both electrodes after activation. The DS-NiSi/n-Si photoanode exhibited a very low photocurrent onset potential of 1.03 V vs RHE, which was 280 mV lower than that of the 1.31 V vs RHE obtained from the NiSi/n-Si photoanode. The large negative shift of the photocurrent onset potential could be attributed to the increase of the photovoltage. It is known that the difference between the electrochemical open circuit potentials (OCPs) of a photoelectrode in the dark and under illumination could reveal its photovoltage.[22] Therefore, the OCPs of the NiSi/n-Si and DS-NiSi/n-Si in the dark and under illumination were employed to determine the respective photovoltages. As shown in Figure 4b, the difference in OCPs in the dark and under illumination was increased from 140 mV for NiSi/n-Si to 400 mV for DS-NiSi/n-Si. That means the photovoltage of DS-NiSi/n-Si is 260 mV higher than that of NiSi/n-Si, which shows an agreement with the results of the CV measurement. The large photovoltage of DS-NiSi/n-Si compared to that of NiSi/n-Si was attributed to the high SBH of DS-NiSi/n-Si. In a Schottky junction (MS or MIS) device, the photovoltage scales linearly with the SBH.[39] The high SBH of the DS-NiSi/n-Si of 0.94 eV indicates the strong band bending of Si and the formation of a large built-in electric field at the Si surface. Consequently, a high photovoltage and a low photocurrent onset potential were achieved due to the associated enhancement in the separation of the photoinduced electron−hole pairs.

In addition, both samples exhibited high saturated photocurrent densities of 33 mA cm^{-2}, which was ascribed to the highly efficient charge transport in this configuration. First, the full avoidance of a disordered native SiO_2 layer in the present

https://dx.doi.org/10.1021/acsami.0c09498
ACS Appl. Mater. Interfaces 2020, 12, 39092−39097

photoanodes configuration and the metallic nature of NiSi could facilitate the transport of the photoinduced holes from substrate Si to the electrode surface. Second, it is known that a highly efficient catalyst, which accelerates the injection of photoinduced holes from the electrode surface into the electrolyte, was also critical for high photocurrent densities during the oxidation of water.[21] XPS and depth profiling experiments using Ar^+ sputtering were employed to observe the composition of the NiSi/n-Si photoanode under different conditions (Note S2, Supporting Information). The high-resolution Ni $2p_{2/3}$ spectra are shown in Figure 4c. For the as-prepared sample, the XPS data show a native oxide phase of Ni on the surface of the NiSi film.[40,41] After activation, the peaks corresponding to nickel oxyhydroxide (NiOOH) appeared,[42] which indicates the formation of NiOOH on the NiSi film during activation in 1 M KOH solution. The NiOOH as a highly active OER catalyst improves the kinetics of the OER at the electrode surface.[43] After Ar^+ sputtering took place on the activated sample for 30 s, the peaks corresponding to the NiOOH disappeared, while peaks corresponding to NiSi appeared, which indicated that the NiOOH was present only on the surface, and the material underneath was still bulk NiSi after the activation of the NiSi film. Obviously, the metallic NiSi had the synergic advantages of high electrical conductivity and OER catalytic activity after activation. Linear sweep voltammetry measurements were performed both in 1 M KOH and 1 M KOH + 1 M Na_2SO_3 solution to calculate the separation and injection efficiency of DS-NiSi/n-Si photoanode.[44] The results are shown in Figure S3a,b. The photoanode exhibits a high injection efficiency of above 90% and separation efficiency of above 80% at saturation voltage. As summarized in Table S1, the DS-NiSi/n-Si photoanode with a simple MS Schottky junction structure exhibited excellent PEC water-splitting performance.

Furthermore, the PEC stability of the DS-NiSi/n-Si was investigated by chronoamperometry carried out at a constant potential of 1.7 V vs RHE in 1 M KOH solution. The results are shown in Figure 5a. There is no noticeable decay of the photocurrent during continuous operation for 20 h, which implies that the DS-NiSi/n-Si photoanode has high PEC stability. The CV curves of the DS-NiSi/n-Si revealed that the photoanode retained its high PEC activity after 20-h tests (Figure 5b). The redox peaks in the CV curves correspond to the $Ni^{2+/3+}$ redox reaction.[43,45] The increase of the peaks area and the positive shift of the peaks could be attributed to additional formation of NiOOH during the stability test.[45] It is reported that NiSi can be used as a competent mask material for selective Si etching in KOH.[46] The strong alkali corrosion resistance of NiSi (or NiSi/NiOOH) film enables the photoanode to have high stability during the PEC operation in alkaline solution.

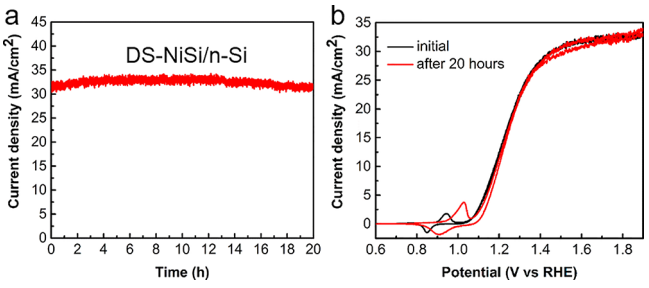

Figure 5. (a) Chronoamperometric current densities versus time curves of the DS-NiSi/n-Si measured at a constant applied potential of 1.7 V vs RHE in 1 M KOH solution under simulated 100 mW cm^{-2} illumination. (b) CV curves of DS-NiSi/n-Si before (black) and after (red) a 20-h stability test.

CONCLUSIONS

In summary, we have successfully fabricated a high-performance NiSi/n-Si MS Schottky junction photoanode by employing metal silicidation in conjunction with DS. Through metal silicidation, a high-quality NiSi/n-Si interface without a disordered native SiO_2 layer was obtained, which ensures highly efficient charge transport. The subsequent DS gives the photoanode a high SBH through the introduction of electric dipoles at the NiSi/n-Si interface, and thereby, a high photovoltage was achieved. After activation in 1 M KOH solution, the NiSi/n-Si photoanode exhibited a high saturated photocurrent density of 33 mA cm^{-2} and a low onset potential of 1.03 V vs RHE. In addition, the strong alkali corrosion resistance of NiSi endows the photoanode with high stability during PEC operation in 1 M KOH. In future, this metal silicidation in conjunction with the DS strategy could be applied to the fabrication of other metal−silicides/Si photoanodes and photocathodes.

ASSOCIATED CONTENT

Supporting Information

The Supporting Information is available free of charge at https://pubs.acs.org/doi/10.1021/acsami.0c09498.

Electrochemical impedance spectroscopy and Mott−Schottky analysis, XPS analysis, microscopic images, calculation methods, and photoelectrochemical measurements (PDF)

AUTHOR INFORMATION

Corresponding Authors

Guangwei She − *Key Laboratory of Photochemical Conversion and Optoelectronic Materials, Technical Institute of Physics and Chemistry, Chinese Academy of Sciences, Beijing 100190, China;* orcid.org/0000-0003-1017-5456; Email: shegw@mail.ipc.ac.cn

Jun Luo − *University of Chinese Academy of Sciences, Chinese Academy of Sciences, Beijing 100049, China; Key Laboratory of Microelectronic Devices & Integrated Technology, Institute of Microelectronics, Chinese Academy of Sciences, Beijing 100029, China;* Email: luojun@ime.ac.cn

Wensheng Shi − *Key Laboratory of Photochemical Conversion and Optoelectronic Materials, Technical Institute of Physics and Chemistry, Chinese Academy of Sciences, Beijing 100190, China; University of Chinese Academy of Sciences, Chinese Academy of Sciences, Beijing 100049, China;* orcid.org/0000-0001-5747-4862; Email: shiws@mail.ipc.ac.cn

Authors

Shengyang Li − *Key Laboratory of Photochemical Conversion and Optoelectronic Materials, Technical Institute of Physics and Chemistry, Chinese Academy of Sciences, Beijing 100190, China; University of Chinese Academy of Sciences, Chinese Academy of Sciences, Beijing 100049, China*

Jing Xu − *Key Laboratory of Microelectronic Devices & Integrated Technology, Institute of Microelectronics, Chinese Academy of Sciences, Beijing 100029, China*

https://dx.doi.org/10.1021/acsami.0c09498
ACS Appl. Mater. Interfaces 2020, 12, 39092−39097

Shaoyang Zhang − *Key Laboratory of Photochemical Conversion and Optoelectronic Materials, Technical Institute of Physics and Chemistry, Chinese Academy of Sciences, Beijing 100190, China; University of Chinese Academy of Sciences, Chinese Academy of Sciences, Beijing 100049, China*

Haoyue Zhang − *Key Laboratory of Photochemical Conversion and Optoelectronic Materials, Technical Institute of Physics and Chemistry, Chinese Academy of Sciences, Beijing 100190, China; University of Chinese Academy of Sciences, Chinese Academy of Sciences, Beijing 100049, China*

Lixuan Mu − *Key Laboratory of Photochemical Conversion and Optoelectronic Materials, Technical Institute of Physics and Chemistry, Chinese Academy of Sciences, Beijing 100190, China;* orcid.org/0000-0002-6613-5368

Chen Ge − *Beijing National Laboratory for Condensed Matter Physics, Institute of Physics, Chinese Academy of Sciences, Beijing 100190, China;* orcid.org/0000-0002-8093-940X

Kuijuan Jin − *Beijing National Laboratory for Condensed Matter Physics, Institute of Physics, Chinese Academy of Sciences, Beijing 100190, China;* orcid.org/0000-0002-0047-4375

Complete contact information is available at: https://pubs.acs.org/10.1021/acsami.0c09498

Notes

The authors declare no competing financial interest.

■ ACKNOWLEDGMENTS

This work was supported by the National Key R&D Program of China (2016YFA0200800; 2017YFE0196400; 2017YFA0303604), NSFC (51672284, 21975269, 11721404, 11674385), Beijing Natural Science Foundation (2181002), Chinese Academy of Sciences (1A1111KYSB20180017, QYZDJ-SSW-JSC032, XDB17000000), and the Youth Innovation Promotion Association of CAS (Grant No. 2015097).

■ REFERENCES

(1) Chu, S.; Cui, Y.; Liu, N. The Path Towards Sustainable Energy. *Nat. Mater.* **2017**, *16* (1), 16−22.

(2) Luo, Z.; Wang, T.; Gong, J. Single-Crystal Silicon-based Electrodes for Unbiased Solar Water Splitting: Current Status and Prospects. *Chem. Soc. Rev.* **2019**, *48* (7), 2158−2181.

(3) Reece, S. Y.; Hamel, J. A.; Sung, K.; Jarvi, T. D.; Esswein, A. J.; Pijpers, J. J. H.; Nocera, D. G. Wireless Solar Water Splitting Using Silicon-Based Semiconductors and Earth-Abundant Catalysts. *Science* **2011**, *334* (6056), 645−648.

(4) Ji, L.; Hsu, H.-Y.; Li, X.; Huang, K.; Zhang, Y.; Lee, J. C.; Bard, A. J.; Yu, E. T. Localized Dielectric Breakdown and Antireflection Coating in Metal-Oxide-Semiconductor Photoelectrodes. *Nat. Mater.* **2017**, *16* (1), 127−131.

(5) Hill, J. C.; Landers, A. T.; Switzer, J. A. An Electrodeposited Inhomogeneous Metal-Insulator-Semiconductor Junction for Efficient Photoelectrochemical Water Oxidation. *Nat. Mater.* **2015**, *14* (11), 1150−1155.

(6) Oh, K.; Mériadec, C.; Lassalle-Kaiser, B.; Dorcet, V.; Fabre, B.; Ababou-Girard, S.; Joanny, L.; Gouttefangeas, F.; Loget, G. Elucidating the Performance and Unexpected Stability of Partially Coated Water-Splitting Silicon Photoanodes. *Energy Environ. Sci.* **2018**, *11*, 2590.

(7) Hemmerling, J.; Quinn, J.; Linic, S. Quantifying Losses and Assessing the Photovoltage Limits in Metal-Insulator-Semiconductor Water Splitting Systems. *Adv. Energy Mater.* **2020**, *10*, 1903354.

(8) Moench, W. On the Alleviation of Fermi-level Pinning by Ultrathin Insulator Layers in Schottky Contacts. *J. Appl. Phys.* **2012**, *111* (7), 073706.

(9) Esposito, D. V.; Levin, I.; Moffat, T. P.; Talin, A. A. H2 Evolution at Si-based Metal-Insulator-Semiconductor Photoelectrodes Enhanced by Inversion Channel Charge Collection and H Spillover. *Nat. Mater.* **2013**, *12* (6), 562−568.

(10) Kim, H.; McIntyre, P. C.; Chui, C. O.; Saraswat, K. C.; Stemmer, S. Engineering Chemically Abrupt High-k Metal Oxide/Silicon Interfaces Using an Oxygen-gettering Metal Overlayer. *J. Appl. Phys.* **2004**, *96* (6), 3467−3472.

(11) Ros, C.; Carretero, N. M.; David, J.; Arbiol, J.; Andreu, T.; Morante, J. R. Insight into the Degradation Mechanisms of Atomic Layer Deposited TiO2 as Photoanode Protective Layer. *ACS Appl. Mater. Interfaces* **2019**, *11* (33), 29725−29735.

(12) Labrador, N. Y.; Li, X.; Liu, Y.; Tan, H.; Wang, R.; Koberstein, J. T.; Moffat, T. P.; Esposito, D. V. Enhanced Performance of Si MIS Photocathodes Containing Oxide Coated Nanoparticle Electrocatalysts. *Nano Lett.* **2016**, *16* (10), 6452−6459.

(13) Loget, G.; Meriadec, C.; Dorcet, V.; Fabre, B.; Vacher, A.; Fryars, S.; Ababou-Girard, S. Tailoring the Photoelectrochemistry of Catalytic Metal-Insulator-Semiconductor (MIS) Photoanodes by a Dissolution Method. *Nat. Commun.* **2019**, *10*, 3522.

(14) Chen, Y. W.; Prange, J. D.; Duhnen, S.; Park, Y.; Gunji, M.; Chidsey, C. E.; McIntyre, P. C. Atomic Layer-deposited Tunnel Oxide Stabilizes Silicon Photoanodes for Water Oxidation. *Nat. Mater.* **2011**, *10* (7), 539−544.

(15) Yu, Y.; Zhang, Z.; Yin, X.; Kvit, A.; Liao, Q.; Kang, Z.; Yan, X.; Zhang, Y.; Wang, X. Enhanced Photoelectrochemical Efficiency and Stability Using a Conformal TiO2 Film on a Black Silicon Photoanode. *Nat. Energy* **2017**, *2*, 17045.

(16) Scheuermann, A. G.; Lawrence, J. P.; Kemp, K. W.; Ito, T.; Walsh, A.; Chidsey, C. E.; Hurley, P. K.; McIntyre, P. C. Design Principles for Maximizing Photovoltage in Metal-Oxide-Protected Water-Splitting Photoanodes. *Nat. Mater.* **2016**, *15* (1), 99−105.

(17) Scheuermann, A. G.; Kemp, K. W.; Tang, K.; Lu, D. Q.; Satterthwaite, P. F.; Ito, T.; Chidsey, C. E. D.; McIntyre, P. C. Conductance and Capacitance of Bilayer Protective Oxides for Silicon Water Splitting Anodes. *Energy Environ. Sci.* **2016**, *9* (2), 504−516.

(18) Scheuermann, A. G.; Prange, J. D.; Gunji, M.; Chidsey, C. E. D.; McIntyre, P. C. Effects of Catalyst Material and Atomic Layer Deposited TiO2 Oxide Thickness on the Water Oxidation Performance of Metal−Insulator−Silicon Anodes. *Energy Environ. Sci.* **2013**, *6* (8), 2487.

(19) Scheuermann, A. G.; Lu, D. Q.; Ito, T.; Chidsey, C. E. D.; McIntyre, P. C., The Effect of SPA-SiO2 Tunnel Oxide Thickness for Metal-Insulator-Silicon Photoelectrochemical Cells. In *Atomic Layer Deposition Applications 10*; Roozeboom, F., DeGendt, S., Delabie, A., Elam, J. W., Londergan, A., VanDerStraten, O., Eds.; The Electrochemical Society: 2014; Vol. *64*, pp 265−276.

(20) Seo, K.-I.; Lee, D.-I.; Pianetta, P.; Kim, H.; Saraswat, K. C.; McIntyre, P. C. Chemical States and Electrical Properties of a High-k Metal Oxide/Silicon Interface with Oxygen-gettering Titanium-Metal-Overlayer. *Appl. Phys. Lett.* **2006**, *89* (14), 142912.

(21) Yao, T.; Chen, R.; Li, J.; Han, J.; Qin, W.; Wang, H.; Shi, J.; Fan, F.; Li, C. Manipulating the Interfacial Energetics of n-type Silicon Photoanode for Efficient Water Oxidation. *J. Am. Chem. Soc.* **2016**, *138* (41), 13664−13672.

(22) Digdaya, I. A.; Adhyaksa, G. W. P.; Trzesniewski, B. J.; Garnett, E. C.; Smith, W. A. Interfacial Engineering of Metal-Insulator-Semiconductor Junctions for Efficient and Stable Photoelectrochemical Water Oxidation. *Nat. Commun.* **2017**, *8*, 15968.

(23) Zheng, J.; Lyu, Y.; Wang, R.; Xie, C.; Zhou, H.; Jiang, S. P.; Wang, S. Crystalline TiO2 Protective Layer with Graded Oxygen Defects for Efficient and Stable Silicon-based Photocathode. *Nat. Commun.* **2018**, *9* (1), 3572.

(24) Laskowski, F. A. L.; Oener, S. Z.; Nellist, M. R.; Gordon, A. M.; Bain, D. C.; Fehrs, J. L.; Boettcher, S. W. Nanoscale Semiconductor/

Catalyst Interfaces in Photoelectrochemistry. *Nat. Mater.* **2020**, *19*, 69−76.
(25) Ji, L.; McDaniel, M. D.; Wang, S.; Posadas, A. B.; Li, X.; Huang, H.; Lee, J. C.; Demkov, A. A.; Bard, A. J.; Ekerdt, J. G.; Yu, E. T. A Silicon-based Photocathode for Water Reduction with an Epitaxial SrTiO3 Protection Layer and a Nanostructured Catalyst. *Nat. Nanotechnol.* **2015**, *10* (1), 84−90.
(26) Murarka, S. P. Transition-Metal Silicides. *Annu. Rev. Mater. Sci.* **1983**, *13*, 117−137.
(27) Jiang, Y.-L.; Ru, G.-P.; Lu, F.; Qu, X.-P.; Li, B.-Z.; Yang, S. Ni/Si Solid Phase Reaction Studied by Temperature-dependent Current-Voltage Technique. *J. Appl. Phys.* **2003**, *93* (2), 866−870.
(28) Iwai, H.; Ohguro, T.; Ohmi, S. NiSi Salicide Technology for Scaled CMOS. *Microelectron. Eng.* **2002**, *60* (1−2), 157−169.
(29) Zhang, Z.; Qiu, Z.; Liu, R.; Ostling, M.; Zhang, S.-L. Schottky-Barrier Height Tuning by Means of Ion Implantation Into Preformed Silicide Films Followed by Drive-In Anneal. *IEEE Electron Device Lett.* **2007**, *28* (7), 565.
(30) Luo, J.; Gao, X.; Qiu, Z.-J.; Lu, J.; Wu, D.; Zhao, C.; Li, J.; Chen, D.; Hultman, L.; Zhang, S.-L. Thermal Stability and Dopant Segregation for Schottky Diodes With Ultrathin Epitaxial NiSi2−y. *IEEE Electron Device Lett.* **2011**, *32* (8), 1029−1031.
(31) Qiu, Z.; Zhang, Z.; Ostling, M.; Zhang, S.-L. A Comparative Study of Two Different Schemes to Dopant Segregation at NiSi/Si and PtSi/Si Interfaces for Schottky Barrier Height Lowering. *IEEE Trans. Electron Devices* **2008**, *55* (1), 396−403.
(32) Li, S.; She, G.; Chen, C.; Zhang, S.; Mu, L.; Guo, X.; Shi, W. Enhancing the Photovoltage of Ni/n-Si Photoanode for Water Oxidation through a Rapid Thermal Process. *ACS Appl. Mater. Interfaces* **2018**, *10* (10), 8594−8598.
(33) Zhou, X.; Liu, R.; Sun, K.; Papadantonakis, K. M.; Brunschwig, B. S.; Lewis, N. S. 570 mV Photovoltage, Stabilized n-Si/CoOx Heterojunction Photoanodes Fabricated Using Atomic Layer Deposition. *Energy Environ. Sci.* **2016**, *9* (3), 892−897.
(34) Luo, J.; Qiu, Z.; Zha, C.; Zhang, Z.; Wu, D.; Lu, J.; Åkerman, J.; Östling, M.; Hultman, L.; Zhang, S.-L. Surface-energy Triggered Phase Formation and Epitaxy in Nanometer-thick Ni1−xPtx Silicide Films. *Appl. Phys. Lett.* **2010**, *96* (3), 031911.
(35) Lauwers, A.; Steegen, A.; de Potter, M.; Lindsay, R.; Satta, A.; Bender, H.; Maex, K. Materials Aspects, Electrical Performance, and Scalability of Ni Silicide Towards Sub-0.13 μm Technologies. *J. Vac. Sci. Technol., B: Microelectron. Process. Phenom.* **2001**, *19* (6), 2026.
(36) Luo, J.; Qiu, Z.-J.; Deng, J.; Zhao, C.; Li, J.; Wang, W.; Chen, D.; Wu, D.; Ostling, M.; Ye, T.; Zhang, S.-L. Variation of Schottky Barrier Height Induced by Dopant Segregation Monitored by Contact Resistivity Measurements. *Microelectron. Eng.* **2014**, *120*, 174−177.
(37) Blum, I.; Portavoce, A.; Hoummada, K.; Tellouche, G.; Chow, L.; Mangelinck, D.; Carron, V. Dopant Diffusivity and Solubility in Nickel Silicides. *Physica Status Solidi (c)* **2011**, *8* (3), 670−673.
(38) Yamauchi, T.; Kinoshita, A.; Tsuchiya, Y.; Koga, J.; Kato, K. 1 nm NiSi/Si Junction Design Based on First-principles Calculation for Ultimately Low Contact Resistance. *2006 IEDM Technol. Dig.* **2006**, 1−4.
(39) Kenney, M. J.; Gong, M.; Li, Y.; Wu, J. Z.; Feng, J.; Lanza, M.; Dai, H. High-performance Silicon Photoanodes Passivated with Ultrathin Nickel films for Water Oxidation. *Science* **2013**, *342* (6160), 836−840.
(40) Nesbitt, H. W.; Legrand, D.; Bancroft, G. M. Interpretation of Ni2p XPS Spectra of Ni Conductors and Ni Insulators. *Phys. Chem. Miner.* **2000**, *27* (5), 357−366.
(41) Wagner, C. D.; Riggs, W. M.; Davis, L. E.; Moulder, J. F.; Muilenberg, G. E. *Handbook of X-ray Photoelectron Spectroscopy. A Reference Book of Standard Data for Use in X-ray Photoelectron Spectroscopy*; Perkin-Elmer Corporation: Eden Prairie, MN, 1979; p 80.
(42) Laskowski, F. A. L.; Nellist, M. R.; Venkatkarthick, R.; Boettcher, S. W. Junction Behavior of n-Si Photoanodes Protected by Thin Ni Elucidated from Dual Working Electrode Photoelectrochemistry. *Energy Environ. Sci.* **2017**, *10* (2), 570−579.
(43) Trotochaud, L.; Ranney, J. K.; Williams, K. N.; Boettcher, S. W. Solution-Cast Metal Oxide Thin Film Electrocatalysts for Oxygen Evolution. *J. Am. Chem. Soc.* **2012**, *134* (41), 17253−17261.
(44) Kim, T. W.; Choi, K. S. Nanoporous BiVO4 Photoanodes with Dual-layer Oxygen Evolution Catalysts for Solar Water Splitting. *Science* **2014**, *343* (6174), 990−994.
(45) Wehrens-Dijksma, M.; Notten, P. H. L. Electrochemical Quartz Microbalance characterization of Ni(OH)2-based Thin Film Electrodes. *Electrochim. Acta* **2006**, *51* (18), 3609−3621.
(46) Bhaskaran, M.; Sriram, S.; Sim, L. W. Nickel Silicide Thin Films as Masking and Structural Layers for Silicon Bulk Micro-machining by Potassium Hydroxide Wet Etching. *J. Micromech. Microeng.* **2008**, *18* (9), 095002.

https://dx.doi.org/10.1021/acsami.0c09498
ACS Appl. Mater. Interfaces 2020, 12, 39092−39097